The Histamine *N*-Methyltransferase T105I Polymorphism Affects Active Site Structure and Dynamics†

Karen Rutherford,‡ W. W. Parson,‡ and Valerie Daggett*,‡,§

Departments of Biochemistry and Bioengineering, University of Washington, Box 355061, Seattle, Washington 98195-5061

Received August 26, 2007; Revised Manuscript Received November 14, 2007

ABSTRACT: Histamine *N*-methyltransferase (HNMT) is the primary enzyme responsible for inactivating histamine in the mammalian brain. The human *HNMT* gene contains a common threonine-isoleucine polymorphism at residue 105, distal from the active site. The 105I variant has decreased activity and lower protein levels than the 105T protein. Crystal structures of both variants have been determined but reveal little regarding how the T105I polymorphism affects activity. We performed molecular dynamics simulations for both 105T and 105I at 37 °C to explore the structural and dynamic consequences of the polymorphism. The simulations indicate that replacing Thr with the larger Ile residue leads to greater burial of residue 105 and heightened intramolecular interactions between residue 105 and residues within helix α3 and strand *β*3. This altered, tighter packing is translated to the active site, resulting in the reorientation of several cosubstrate-binding residues. The simulations also show that the hydrophobic histamine-binding domain in both proteins undergoes a large-scale breathing motion that exposes key catalytic residues and lowers the hydrophobicity of the substrate-binding site.

Histamine is a neurotransmitter and neuromodulator that plays important roles in regulating inflammatory and allergic responses (*2*, *3*), gastric acid secretion (*4*, *5*), and memory and learning (*6*−*8*). Defects in the histaminergic system have been linked with cognitive deficiencies in neurodegenerative diseases, including Alzheimer's disease and Down syndrome (*9*−*12*).

Histamine *N*-methyltransferase (HNMT,[1] EC 2.1.1.8) is the primary enzyme responsible for histamine metabolism in the mammalian brain (*13*−*16*). The human *HNMT* gene contains a common single-nucleotide polymorphism (SNP) that encodes either threonine (T or Thr) or isoleucine (I or Ile) at residue 105 (rs1801105) (*17*). The 105I allele is present in 10−15% of the Caucasian population and ∼6% of the Han Chinese population (*17*−*20*). Replacing T105 with isoleucine results in a lower enzymatic activity and decreased levels of immunoreactive protein in vivo (*17*, *21*−*24*). The apparent K_M values for histamine and cosubstrate *S*-adenosylmethionine (SAM) are 1.3- and 1.8-fold higher, respectively, in the 105I variant than in the 105T protein (*22*). The T105I polymorphism was initially thought to be associated with an increased risk of asthma and inflammation (*25*). However, recent studies have shown no link between the 105I allele and asthma (*26*−*28*) or gastric inflammation (*29*). Interestingly, it is the more active 105T protein that appears to be associated with disease. Two recent studies suggest that the 105I allele confers protection against alcoholism (*30*, *31*). The elevated levels of histamine present in individuals carrying the 105I allele may also provide protection against infectious agents as well as affect anxiety levels, cognition, and sedation (*10*, *11*, *30*).

Several crystal structures of human 105T and 105I HNMT with bound *S*-adenosylhomocysteine (SAH) and a diverse set of inhibitors have been determined (*22*, *32*), revealing a two-domain structure (Figure 1A). The larger domain consists of the highly conserved SAM-binding fold present in many SAM-dependent methyltransferases (Figure 1B). Elements from both the amino and carboxy termini form the hydrophobic substrate-binding domain, which buries histamine substrates in a pocket lined with 14 aromatic residues (Figure 1C). The T105I polymorphism is ∼16 Å from the active site in a loop between helix α4 and strand *β*3, both of which have SAM-binding residues at their distal ends (Figure 1). The root-mean-square deviation of Cα atoms (Cα-rmsd) between the 105T and 105I structures is 0.4 Å. The largest deviations are in the polymorphic loop region (residues 104−110), which has larger crystallographic *B*-factors in 105I HNMT. Residue 105 interacts with the same residues in both variants, the sole exception being the loss of a hydrogen bond between the hydroxyl group of T105 and the backbone carbonyl L101 in the 105I protein. Both proteins interact with cosubstrate SAH in an identical manner.

† Financial support for this work was provided by the National Institutes of Health (Grant GM 50789 to V.D.) and the Canadian Institutes of Health (Grant DRA MD-75910 to K.R.). Figures were produced using the USCF Chimera package from the Computer Graphics Laboratory, University of California, San Francisco (supported by NIH Grant P41 RR-01081).

* To whom correspondence should be addressed. Phone: (206) 685-1510. E-mail: daggett@u.washington.edu.

‡ Department of Biochemistry.

§ Department of Bioengineering.

[1] Abbreviations: HNMT, histamine *N*-methyltransferase; SNP, single-nucleotide polymorphism; SAM, *S*-adenosylmethionine; SAH, *S*-adenosylhomocysteine; 2PM, diphenhydramine; COMT, catechol *O*-methyltransferase; MD, molecular dynamics; SASA, solvent-accessible surface area; Cα-rmsd, Cα root-mean-square deviation from the starting structure; Cα-rmsf, Cα root-mean-square fluctuation about the mean structure.

10.1021/bi701737f CCC: $40.75
Published on Web 12/23/2007

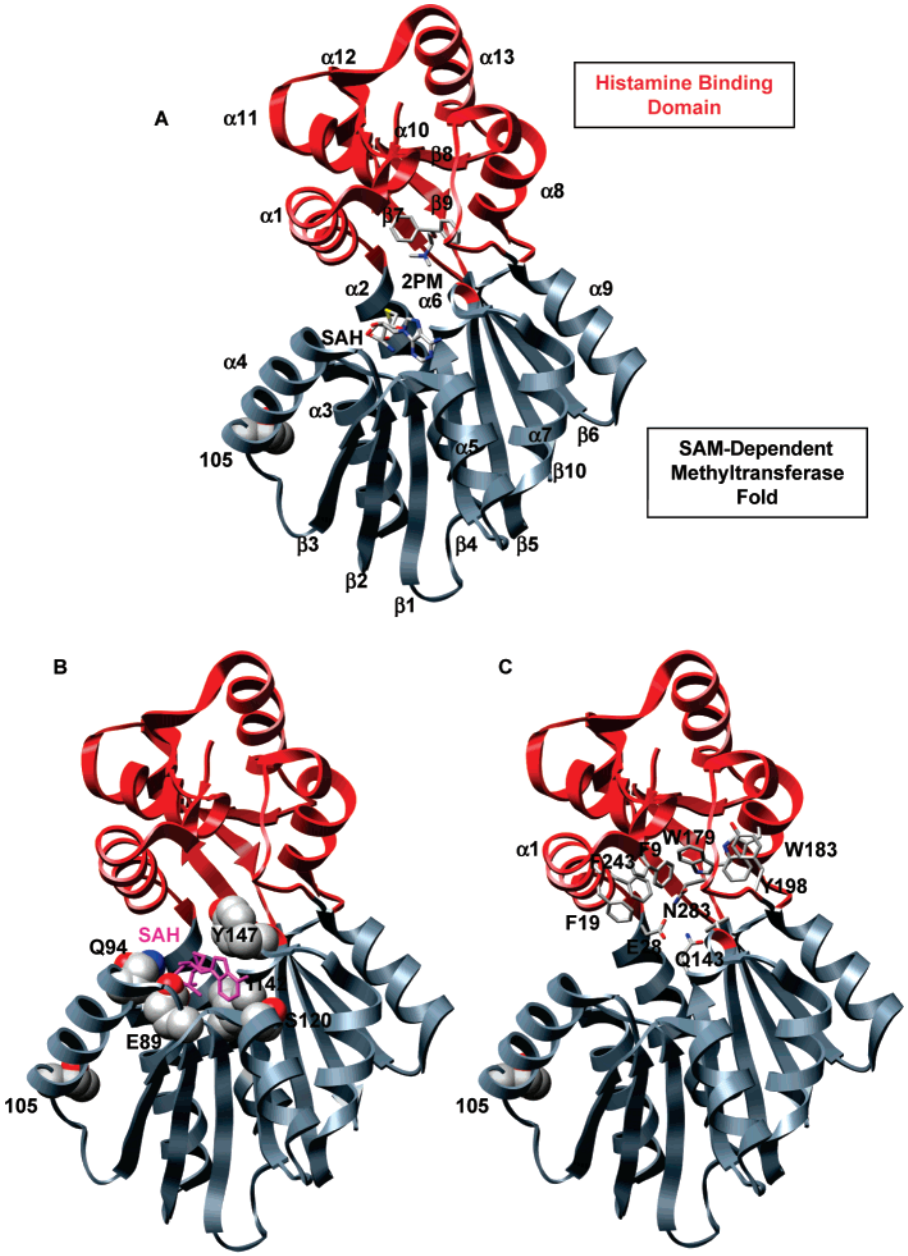

FIGURE 1: Bidomain structure of histamine *N*-methyltransferase. (A) Ribbon diagram of HNMT (2AOT) with the SAM- and histamine-binding domains colored gray and red, respectively. Product SAH, inhibitor diphenhydramine (2PM), and polymorphic residue 105 are colored by atom. (B) Key residues in the highly conserved SAM-dependent methyltransferase domain. SAM interacts with residues from α4 (Q94), α5 (S120), *β*2 (E89 and P90), *β*3 (T119), and *β*4 (I142 and M144). SAH is colored magenta and shown in licorice representation, and residues are colored by atom type and shown in space-filling representation. (C) Key residues in the histamine-binding domain. A trio of catalytic residues (E28, Q143, and N283) is involved in the N-methylation of HNMT substrates. The substrate is buried in a hydrophobic pocket lined with aromatic residues (shown in licorice representation).

The static crystal structures of 105T and 105I HNMT reveal little with regard to how the T105I polymorphism affects substrate binding or catalysis. Therefore, we have performed multiple molecular dynamics (MD) simulations with 105T and 105I HNMT at 37 °C to examine the dynamic and structural consequences of the T105I polymorphism. The simulations show that the hydrophobic histamine-binding domains of both proteins undergo a breathing motion, exposing the catalytic residues and consequently providing a less hydrophobic site for substrate docking. Overall, this motion is more restricted in 105I HNMT, and the Ile variant remains more compact. The larger Ile residue is buried to a greater extent than 105T and interacts with more of the surrounding residues in α3 and *β*4. This altered packing is transmitted directly to the SAM-binding site through α3 and *β*4, resulting in the reorientation of several key catalytic residues at their distal ends.

METHODS

Protein Preparation. Studies have reported that the T105I HNMT polymorphism affects both substrate binding and thermal stability. However, the crystal structures of 105T and 105I HNMT show no differences in their respective active sites. Simulations of the 105T and 105I HNMT apoproteins were therefore essential for studying the effects of residue 105 on overall HNMT structure and dynamics. Because no crystal structures of the HNMT apoproteins are available, chain A of a 1.9 Å crystal structure of human 105T

histamine *N*-methyltransferase [PDB entry 2AOT (*32*), residues 5−292] bound with SAH and diphenhydramine (2PM) was the starting structure for all of the simulations. The substrate molecules were removed, and *S*-hydroxycysteine was replaced with cysteine at positions 82, 217, and 248. The T105I variant was generated by replacing Thr 105 with Ile and minimizing the torsional, electrostatic, and van der Waals potential energy of the resultant structure in vacuo (*33*). We chose not to use one of the T105I crystal structures because in one case the resolution is too low (3 Å) and the other is a 1.9 Å structure but contains unknown atoms and is missing density for α1.

Molecular Dynamics Simulations. Molecular dynamics (MD) simulations of the 105T and 105I HNMT proteins were performed with the *in lucem* molecular mechanics (*il*mm) simulation package (*34*) using protocols described elsewhere (*34*−*37*). The simulations included all hydrogen atoms and explicit flexible three-centered waters (*37*). The proteins were solvated in a rectangular box with walls extending at least 10 Å from any protein atom. Solvent densities were set to 0.997 and 0.933 g/mL for simulations performed at 25 and 37 °C, respectively (*38*). After the densities had been set, the box volume was held fixed and the NVE microcanonical ensemble was employed. A 10 Å force-shifted, nonbonded cutoff was used, and it was updated every two steps. The potential energy function and associated methods have been described previously (*33*−*36*). A time step of 2 fs was used in all calculations. All simulations were run for 21 ns, and structures were saved every 1 ps for analysis. One 25 °C simulation and three independent 37 °C simulations were performed for each system for a total of 84 ns of simulation time for each protein.

Analyses. Average Cα-rmsds, solvent-accessible surface areas (SASAs), and contact distances were calculated using structures from the last 5 ns (5000 structures) of each simulation. SASA was determined using in-house software by implementing the NACCESS algorithm (*39*). A contact was defined as a C−C atom distance of ≤5.4 Å or a heavy atom (O, N, S) distance of ≤4.6 Å between two non-neighboring residues. In Figure 2, Cα-rmsf values for the HNMT crystal structure [PDB entry 2AOT (*32*)] were calculated using crystallographic *B*-factors (*B*) via the equation Cα-rmsf $= [3B/(8\pi^2)]^{1/2}$ (*40*).

The data described in Tables 1−3 are based on sets of three simulations at 37 °C for both 105T and 105I HNMT. The errors are the standard deviations in the average values of the ensembles for each reported property. The statistical significance of the data was determined using the Student's *t* test. Images were created using CHIMERA (*1*).

RESULTS AND DISCUSSION

We ran multiple simulations of both 105T and 105I HNMT to examine the effects of the T105I polymorphism on the structure and dynamics of the protein. The Cα-rmsd between the 105T and 105I HNMT starting structures after energy minimization was 0.4 Å. The overall HNMT structure was maintained throughout all of the simulations, and the polymorphism did not grossly disrupt the protein. However, the structures of both variants expanded and became slightly flattened during the simulations, while their overall solvent-accessible surface area (SASA) increased. This was most likely due to the removal of both the SAH and 2PM substrates (Figure 1). At 37 °C, the SAM- and histamine-binding domains both became more exposed to solvent, and the Cα-rmsd of the SAM-binding domain reached ∼3.5 Å in both proteins (Table 1). However, the histamine-binding domain was significantly more disrupted in the 105T HNMT simulations, reaching a Cα-rmsd of 5.2 ± 0.7 Å compared with a value of 3.7 ± 1.1 Å in the 105I protein.

Figure 2 shows the average Cα root-mean-square fluctuations (Cα-rmsf) about the mean structure for the 37 °C simulations, along with the crystallographic *B*-factors of HNMT [PDB entry 2AOT (*32*)]. The fluctuations during the simulations are of the same magnitude and follow a pattern similar to that of the *B*-factors. The largest Cα-rmsfs were

Table 1: General Properties of the Simulations

	105T HNMT		105I HNMT	
property	initial[g]	37 °C	initial[g]	37 °C
Cα-rmsd of the methyltransferase domain (Å)[a]	NA[h]	3.7 ± 0.8	NA[h]	3.2 ± 0.8
Cα-rmsd of the histamine-binding domain (Å)[b]	NA[h]	5.2 ± 0.7	NA[h]	3.7 ± 1.1[i]
total SASA (Å^2)[c]	13618	16746 ± 568	13596	16064 ± 677
SAM-binding site SASA (Å^2)[d]	289	502 ± 83	288	455 ± 76
histamine-binding site SASA (Å^2)[e]	359	1712 ± 164	354	1096 ± 130[j]
residue 105 SASA (Å)	41.2	59 ± 12	52.0	53 ± 23
polymorphic site SASA (Å^2)[f]	498	431 ± 28	514	460 ± 35

[a] Cα-rmsd values were calculated using structures from the last 5 ns (5000 structures) of each simulation. The Cα-rmsd of the methyltransferase domain was calculated using the Cα atoms of all residues colored gray in Figure 1. All values are expressed as means and standard deviations of the means from three independent simulations at 37 °C. [b] The Cα-rmsd of the histamine-binding domain was calculated using the Cα atoms of all residues colored red in Figure 1. [c] The total solvent-accessible surface area was determined using the NACCESS algorithm (*39*). [d] The following residues were used to calculate the SASA of the SAM-binding site: M32, G60, E89, P90, Q94, T119, S120, I142, M144, and Y147. [e] The following residues were used to calculate the histamine-binding site SASA: F9, F19, F22, Y147, V173, W179, W183, C196, Y198, and F243. [f] The following residues were used to calculate the polymorphic site SASA: L68, L71, S72, L101, K104, S106, N107, L108, V111, F113, and residue 105. [g] Initial refers to the minimized starting structure. [h] Not applicable. [i] $p < 0.1$. [j] $p < 0.025$.

Table 2: Active Site Distances (Å)

	105T HNMT		105I HNMT	
contact pair[a]	initial[b]	37 °C	initial[b]	37 °C
SAM-binding domain				
M32 CE−I142 CG2	3.6	11.3 ± 4.9	3.6	8.8 ± 4.8
P90 CD−T119 CB	5.3	5.0 ± 0.5	5.3	5.9 ± 1.7
P90 CD−M144 CD	8.2	15.0 ± 3.7	8.2	14.8 ± 3.5
Q94 CG−I142 CB	12.7	16.5 ± 3.1	12.7	16.7 ± 3.6
S120 CB−M144 CG	7.1	9.3 ± 3.0	7.1	9.4 ± 2.4
histamine-binding domain				
E28 OE1−Q143 NE2	3.5	16.8 ± 9.2	3.0	12.5 ± 9.0
E28 OE2−N283 ND2	2.7	12.5 ± 5.8	2.7	12.1 ± 5.0
Q143 NE2−N283 ND2	5.7	10.7 ± 2.4	5.8	12.7 ± 3.4
F9 CB−C196 CB	6.7	23.7 ± 3.1	6.7	16.8 ± 6.4
F19 CG−Y147 OH	7.4	20.1 ± 4.7	7.4	15.1 ± 4.4
V173 CG1−F243 CZ	8.6	19.6 ± 2.7	8.6	15.5 ± 4.2
W183 CG−Y198 CG	3.7	5.1 ± 1.1	3.7	4.8 ± 0.6

[a] All values are expressed as means and standard deviations of the mean of three independent simulations at 37 °C. [b] Initial refers to the minimized starting structure.

Table 3: Active Site Residue Solvent Exposure

	side chain SASA (Å^2)[a]			
	105T HNMT		105I HNMT	
	initial[b]	37 °C	initial[b]	37 °C
SAM-binding domain				
E89	10	38 ± 6	10	43 ± 16
P90	56	47 ± 8	56	41 ± 16
Q94	60	47 ± 21	60	56 ± 15
T119	47	53 ± 6	47	50 ± 8
I142	12	44 ± 28	12	45 ± 27
M144	20	49 ± 22	20	62 ± 21
histamine-binding domain				
F9	34	126 ± 41	34	131 ± 35
E28	5	75 ± 38	5	85 ± 30
Q143	30	71 ± 23	30	85 ± 23
N283	1	18 ± 12	1	11 ± 7
Y147	78	104 ± 30	78	105 ± 31
C196	14	30 ± 18	14	32 ± 14
Y198	58	65 ± 16	58	54 ± 16
E246	18	85 ± 20	18	73 ± 28
F243	25	47 ± 23	25	43 ± 13
L285	0	23 ± 17	0	30 ± 16

[a] All values are expressed as means and standard deviations of the mean of three independent simulations at 37 °C. [b] Initial refers to the minimized starting structure.

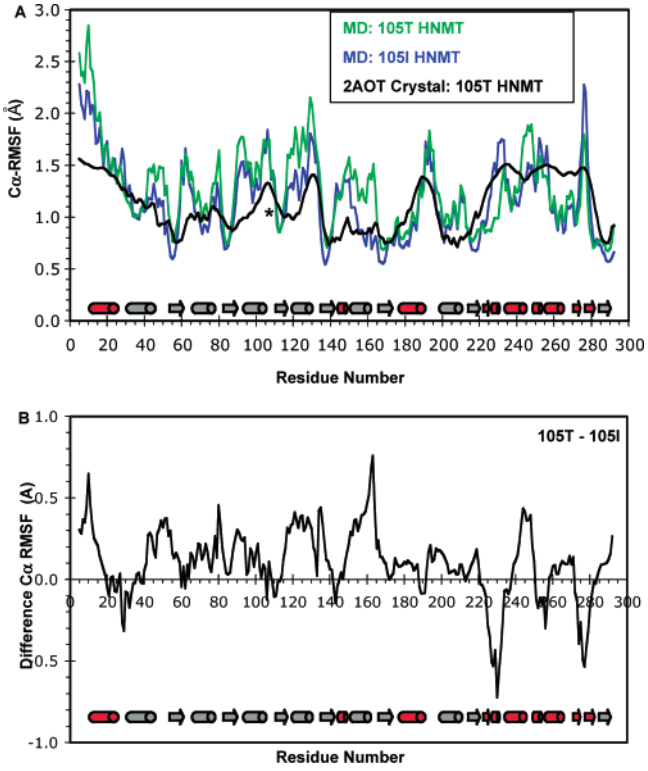

FIGURE 2: Mobility of histamine *N*-methyltransferase. (A) Cα-rmsfs (Å) per residue from the 105T (green) and 105I (blue) MD simulations at 37 °C. Cα-rmsfs were calculated relative to the average structure over the last 10 ns of each simulation. Experimental *B*-factors of the 105T HNMT crystal structure [2AOT (*32*)] are colored black. The asterisk marks residue 105. (B) Cα-rmsf difference plot for the HNMT simulations. Positive and negative values indicate greater overall fluctuations in the 105T and 105I HNMT proteins, respectively. Secondary structural elements are depicted with cylinders for α-helices and arrows for *β*-strands and are colored to match the SAM- and histamine-binding domains shown in Figure 1.

in the helices and loops of both proteins, especially α1, which makes up one face of the histamine-binding domain, α5 (residues 120−130), and the solvent-exposed E276. *β*-Strands positioned within the core of the SAM-binding domain demonstrated the smallest fluctuations (Figure 2A). The Cα-rmsf values differ significantly between the 105T and 105I HNMT simulations at several places within the protein. Residues on the surface of the histamine-binding domain (*β*7 and α10) fluctuated more in the105I HNMT simulations. 105T HNMT exhibited larger fluctuations for residues 145−163 and 243−248, which contain buried core SAM (I142, M144, and Y147) and histamine (Y146, Y147, F243, and E246) binding residues. The Cα-rmsd and Cα-rmsf values suggest that the histamine-binding domain of HNMT is quite flexible (Figure 2B and Table 1).

Substrate Binding and the Inherent Flexibility of the Histamine-Binding Domain. The histamine-binding domain has a mixed α/*β*-structure and is comprised of residues from both the amino and carboxy termini of HNMT. The interior of the domain is lined with 14 aromatic residues, providing a hydrophobic pocket for substrate docking and burial. Three polar residues (E28, Q143, and N283) and several water molecules form a hydrogen-bonded network at the base of the pocket (Figure 1C). These residues interact directly with the substrate's charged residues to both orient the substrate and catalyze its N-methylation (*22*, *32*). In addition, residues C196 and E246 positioned at opposite ends of the pocket are important for substrate binding (*32*). Because HNMT is inhibited by a variety of rigid, aromatic compounds with little structural similarity, it has been hypothesized that the histamine-binding domain exhibits an inherent flexibility that allows tight binding of diverse compounds (*22*, *32*). More importantly, because the bound substrate or inhibitor is completely buried in the crystal structures, the histamine-binding domain must open up for the substrate to enter the active site.

The Cα-rmsd of the histamine-binding domain reached 5.2 Å in simulations of 105T HNMT (Table 1). This deviation was due mainly to the flexibility of α1 (Figures 1 and 2). Several aromatic residues (F9, Y15, F19, and F22) align along one side of α1 to form part of the histamine-binding pocket (Figure 1C). α1 is reoriented and extended during the simulations, separating the domain into two clusters of aromatic residues (Figure 3). Throughout the simulations, α1 and α11 remain in contact via multiple salt bridges and a hydrophobic interaction between F22 and F243, and the two helices move in concert (Figure 4B). A hydrophobic patch (V173, W179, W183, F190, C196, and F243) remains available for substrate binding at the back of the pocket (Figure 3). The motions of α1 open up the histamine-binding domain, increasing the solvent exposure of the active site by ∼1300 Å^2 (Table 1). There also is a large increase in the solvent accessibility of residues E28, Q143, and N283 at the base of the active site (Figure 3 and Table 3). Overall, this open pocket provides a more accessible site for docking an amphipathic substrate than the initial, tightly packed cluster of hydrophobic residues.

Interestingly, α1 appeared to move back toward its starting orientation in several simulations, resulting in a partial repacking of the histamine-binding domain's hydrophobic core (Figures 3 and 4). This cyclical movement was facilitated by the close association of helices α1 and α11 (Figure 4). It is possible that SAM binding affects the motion of α1, as the cosubstrate interacts with several residues (M32,

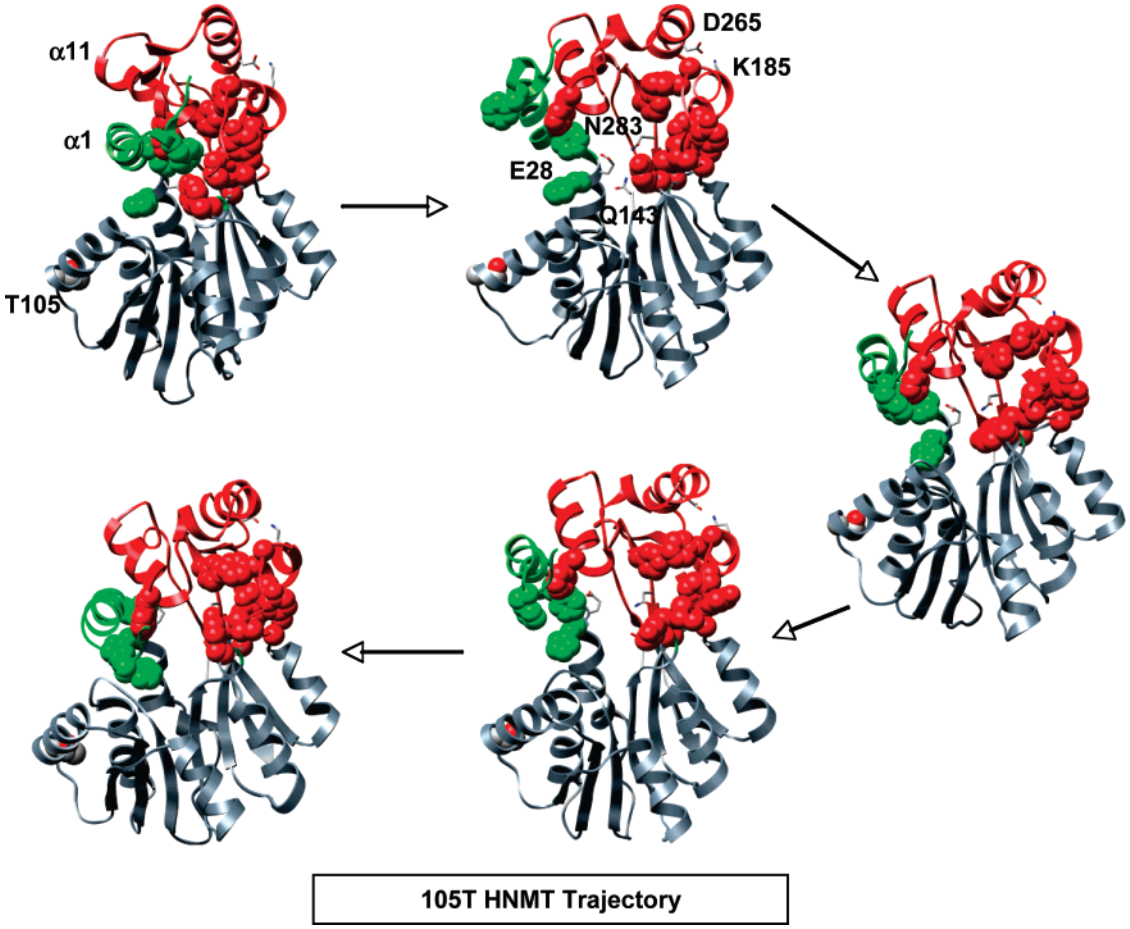

FIGURE 3: Snapshots from a MD simulation of 105T HNMT at 37 °C. α1 elongates, breaking apart the aromatic cluster within the histamine-binding domain and exposing E28, Q143, and N283 to the solvent. Hydrophobic interactions between α1 and α11 and salt bridges throughout the domain allow the hydrophobic cluster to re-form. This breathing motion may facilitate the entry of charged substrates in a highly hydrophobic environment. Hydrophobic residues within the histamine-binding domain are shown in space-filling representation and colored green (α1) and red. The catalytic trio (E28, Q143, and N283) and the K185−D265 salt bridge are colored by atom type and shown in licorice representation.

M144, and Y147) positioned near the histamine-binding domain (Figure 1). Examination of the HNMT crystal structures bound with a diverse set of competitive substrate inhibitors shows that the extent and orientation of contacts between residues in α1 (F9, Y15, F19, and F22) and α6 (Y146 and Y147) and the aromatic moieties of the substrate molecules greatly influence HNMT substrate binding affinity. This periodic opening and closing of the active site would expose both a hydrophobic patch and the catalytic residues necessary for substrate docking and orientation. The α1−α11 arm could then close off the active site, burying the substrate. Further experimental studies that examine the dynamics of helix α1 and HNMT substrate binding are necessary to fully understand how the breathing motion identified here is influenced by both substrate size and the presence of SAM.

Effects of the T105I Polymorphism. Horton et al. (*22*) reported larger crystallographic *B*-factors for the polymorphic loop of 105I HNMT than for the 105T protein (*22*). However, increased flexibility in the residues immediately surrounding I105 was not observed in the simulations (Figure 2). In the initial structures of both 105T and 105I HNMT, residue 105 formed backbone hydrogen bonds with residues in α4 (L101 and V102) and hydrophobic contacts with residues in α3 (L68), α4 (L101, A103, V102, and K104), and the adjacent loop (S106, N107, and L108) (Figure 5A). The additional hydrogen bond formed between the hydroxyl group of T105 and the backbone carbonyl of L101 was maintained throughout the 105T simulations.

The overall solvent exposure of the polymorphic site was similar in all simulations (Table 1); however, large variations in the solvent accessibility of both I105 and its surroundings occurred at 37 °C (Table 1). Residue 105 was buried to a greater extent in the 105I protein, and the larger Ile formed side chain contacts with additional residues in α3 (L71 and S72) and β3 (V111 and F113) that were absent in all of the 105T simulations (Table 1 and Figures 5A and 6B). These packing differences suggest that any changes in the orientation of the smaller Thr side chain are buffered by the additional space present in the polymorphic site and have little effect on the overall protein structure (Figure 5B). In contrast, the more tightly interacting Ile appears to act as a pivot point, affecting the orientation of nearby α3, α4, and β3 through its direct side chain contacts and transmitting these changes to the SAM-binding site (Figure 5). Several residues at the distal ends of α4 (E89, P90, and Q94) and β3 (T119) interact with the adenosine ring of SAM (Figure 1B). Although some of the contact distances and solvent accessibilities of residues within the SAM-binding site remain similar in both proteins (Tables 1−3), many of the

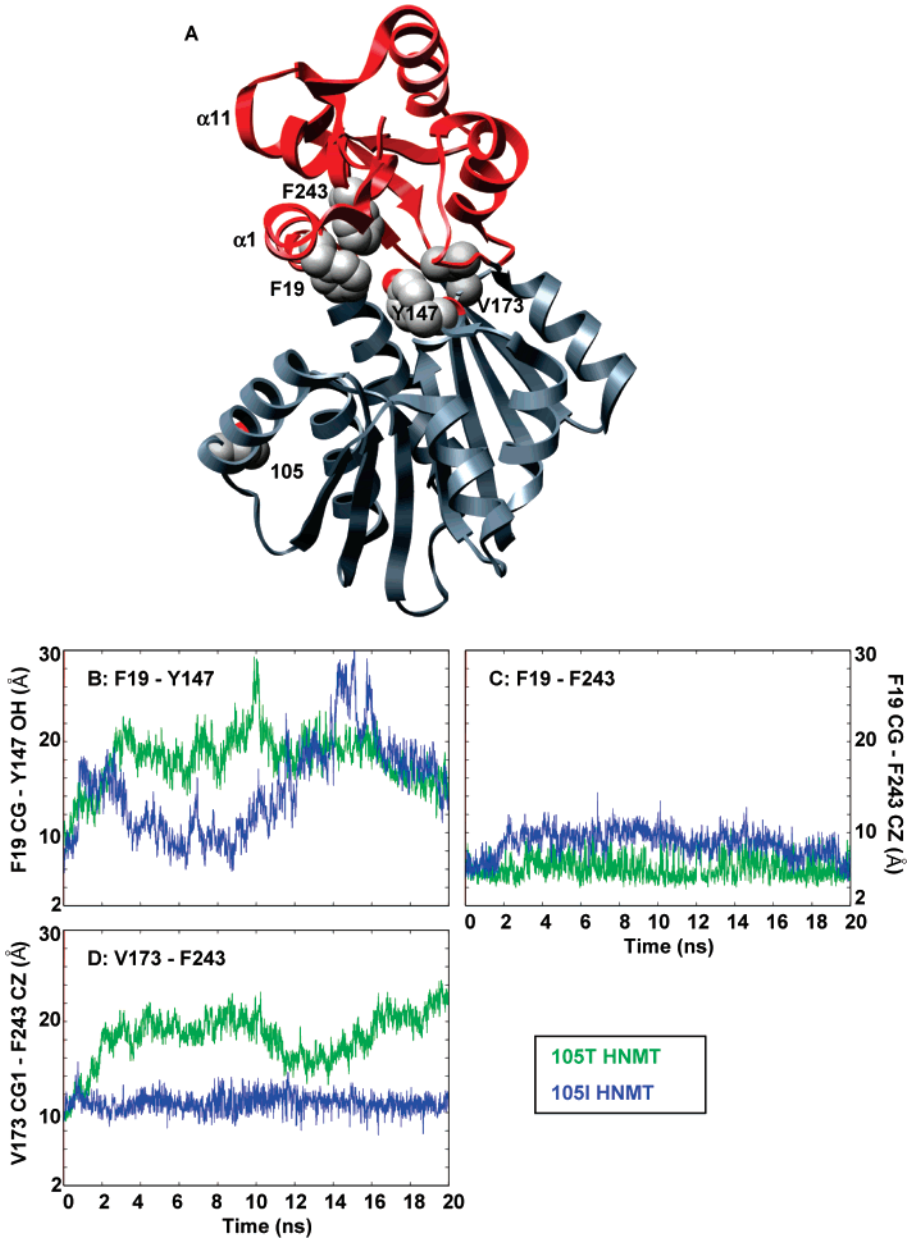

FIGURE 4: Distances between core residues within the histamine-binding domains of 105T and 105I HNMT. The contact distances between core residues within the histamine-binding domain (F19−Y147 and V173−F243) fluctuate greatly with time, reflecting the periodic breathing motion of HNMT that may facilitate substrate binding. The distance between F19 and F243 is more constant throughout the simulations, as α1 and α11 remain in contact and move together. (A) Ribbon diagram of HNMT showing the positions of residues F19, Y147, V173, and F243 within the histamine-binding domain (red). Residue side chains are shown in space-filling representation and colored by atom type. (B) F19 CG (α1)−Y147 OH (α6), (C) F19 CG (α1)−F243 CZ (α11), and (D) V173 CG1 (*β*5)−F243 CZ (α11) contact distances are plotted vs time for the 105T (green) and 105I (blue) HNMT simulations at 37 °C.

SAM-binding residues adjacent to the polymorphic site become more flexible and disordered in the 105I simulations (Figure 3B,C and Tables 2 and 3), which may explain the increase in its apparent K_M for SAM (*22*).

In contrast to the effects on the SAM-binding site, the active site distances and the solvent exposure of residues within the histamine-binding domain are larger and show fluctuations in the 105T HNMT simulations greater than those of the 105I protein (Tables 2 and 3). The additional contacts of I105 that disorder the SAM-binding site may play a role in stabilizing the histamine-binding domain. The larger Ile forms side chain contacts with L68, L71, and S72 in α3 (Figure 5). The reorientation of α3 in the 105I HNMT simulations allows these residues to interact with E28 (α2), a catalytic residue, through I66 (Figure 6C). Neither the I105−L71 interaction nor the E28−I66 interaction occurs in the T105 simulations (Figure 6). The restricted flexibility of this region in 105I HNMT could possibly impair substrate binding, accounting for the slight increase in its apparent K_M for histamine (Table 3) (*22*).

Interestingly, catechol *O*-methyltransferase (COMT), a fellow member of the SAM-dependent methyltransferase fold family, also has a common polymorphism (V108M) that occupies an almost identical position in the COMT tertiary structure as T105I in HNMT (*22*, *32*, *41*). However, unlike T105I in HNMT, the COMT V108M polymorphism appears to result in decreased protein stability (*42*−*44*) and to have little effect on substrate binding (*43*, *45*). MD simulations

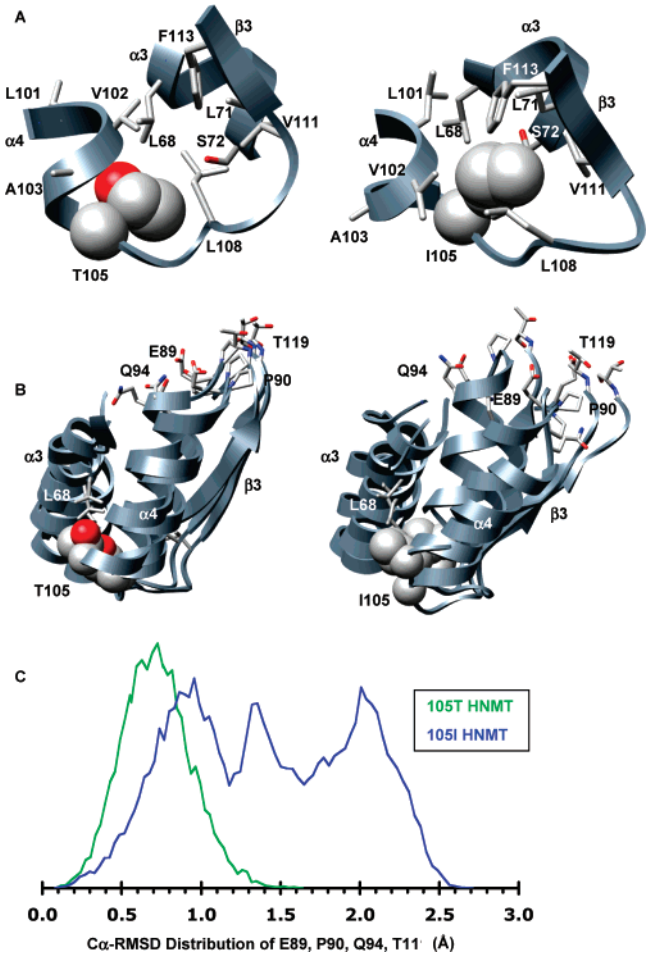

FIGURE 5: Snapshots of polymorphic packing taken from the 20 ns structures of the 105T and 105I HNMT MD simulations at 37 °C. (A) Packing at the polymorphic site. The larger Ile is more buried, forming side chain contacts with residues from α3 (L71 and S72) and β3 (V111 and F113) that are not present in the 105T simulations. (B) Polymorphic packing affects the SAM-binding site. Structural overlay of the polymorphic and SAM-binding sites from the 20 ns structures of three independent simulations of 105T and 105I HNMT. The more tightly packed Ile acts as a pivot point among α3, α4, and β3, disrupting the orientation of key SAM-binding residues (E89, P90, Q94, and T119). The side chain of the polymorphic residue and its contacts are colored by atom type and shown in space-filling and licorice representations, respectively. (C) Distributions of the Cα-rmsds for residues E89, P90, Q94, and T119 during the last 10 ns of all three of the 105T (green) and 105I (blue) HNMT simulations at 37 °C. The SAM-binding residues are more mobile in 105I HNMT, existing in a large ensemble of conformations that differ greatly from their respective positions in the starting structure. The distribution for 105T HNMT is narrower, indicating that the active site structure of 105T HNMT is maintained throughout the simulations. The vertical scales are arbitrary.

of the COMT variants showed that the larger Met formed closer side chain contacts with residues within the polymorphic site, resulting in an increased sensitivity to structural changes in nearby helices and a distortion of the SAM-binding site (*41*). These changes were propagated throughout the protein, resulting in an increase in the overall SASA of 108M COMT, loosening of the active site, and destabilization of the protein.

CONCLUSIONS

The HNMT active site undergoes a breathing motion, periodically exposing a trio of catalytic residues and a core

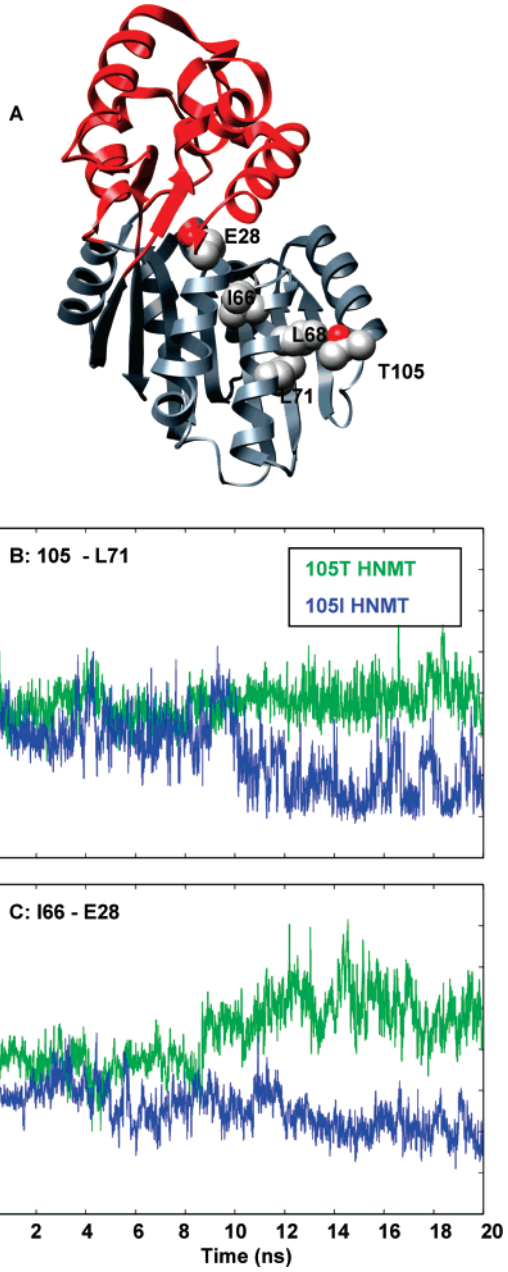

FIGURE 6: Translation of polymorphic packing effects to the histamine-binding site. Secondary structures surrounding the polymorphic residue are more susceptible to changes in orientation caused by altered contacts between L71 and S72 and the larger Ile side chain. These structural changes are translated to the histamine-binding site via a new contact between α3 (I66) and α2 (E28). (A) Ribbon diagram of HNMT showing the location of residues 105, L68, L71, I66, and E28. Side chains are shown in space-filling representation and colored by atom type. (B) 105 CG2−L71 CD2 (α3) and (C) I66 CD1 (α3)−E28 CB (α2, catalytic trio) contact distances for the 105T (green) and 105I (blue) HNMT simulations at 37 °C.

hydrophobic patch important for substrate docking and orientation. Aromatic residues lining the highly flexible α1 then bury the substrate in the enzyme−substrate complex. The identity of residue 105 had a significant effect on active site structure and dynamics, even though they are separated by 16 Å. I105 was buried to a greater extent and consequently contacted more residues within α3 and β3 than did T105. This altered packing reoriented α3 and β3, disordering several key SAM-binding residues on their distal ends while slightly stabilizing the histamine-binding domain.

ACKNOWLEDGMENT

We thank Amanda Jonsson for running the simulations.

REFERENCES

1. Pettersen, E. F., Goddard, T. D., Huang, C. C., Couch, G. S., Greenblatt, D. M., Meng, E. C., and Ferrin, T. E. (2004) UCSF Chimera: A visualization system for exploratory research and analysis, *J. Comput. Chem. 25*, 1605−1612.
2. Rosenwasser, L. (2007) New insights into the pathophysiology of allergic rhinitis, *Allergy Asthma Proc. 28*, 10−15.
3. Zhang, M., Thurmond, R. L., and Dunford, P. J. (2007) The histamine H(4) receptor: A novel modulator of inflammatory and immune disorders, *Pharmacol. Ther. 113*, 594−606.
4. Schubert, M. L. (1999) Regulation of gastric acid secretion, *Curr. Opin. Gastroenterol. 15*, 457.
5. Chen, D., Friis-Hansen, L., Hakanson, R., and Zhao, C. M. (2005) Genetic dissection of the signaling pathways that control gastric acid secretion, *Inflammopharmacology 13*, 201−207.
6. Bacciottini, L., Passani, M. B., Mannaioni, P. F., and Blandina, P. (2001) Interactions between histaminergic and cholinergic systems in learning and memory, *Behav. Brain Res. 124*, 183−194.
7. Passani, M. B., Bacciottini, L., Mannaioni, P. F., and Blandina, P. (2000) Central histaminergic system and cognition, *Neurosci. Biobehav. Rev. 24*, 107−113.
8. Yanai, K., and Tashiro, M. (2007) The physiological and pathophysiological roles of neuronal histamine: An insight from human positron emission tomography studies, *Pharmacol. Ther. 113*, 1−15.
9. Schneider, C., Risser, D., Kirchner, L., Kitzmuller, E., Cairns, N., Prast, H., Singewald, N., and Lubec, G. (1997) Similar deficits of central histaminergic system in patients with Down syndrome and Alzheimer disease, *Neurosci. Lett. 222*, 183−186.
10. Kim, S. H., Cairns, N., Fountoulakisc, M., and Lubec, G. (2001) Decreased brain histamine-releasing factor protein in patients with Down syndrome and Alzheimer's disease, *Neurosci. Lett. 300*, 41−44.
11. Kim, S. H., Krapfenbauer, K., Cheon, M. S., Fountoulakis, M., Cairns, N. J., and Lubec, G. (2002) Human brain cytosolic histamine-N-methyltransferase is decreased in Down syndrome and increased in Pick's disease, *Neurosci. Lett. 321*, 169−172.
12. Fernandez-Novoa, L., and Cacabelos, R. (2001) Histamine function in brain disorders, *Behav. Brain Res. 124*, 213−233.
13. Lortie, M. J., Novotny, W. F., Peterson, O. W., Vallon, V., Malvey, K., Mendonca, M., Satriano, J., Insel, P., Thomson, S. C., and Blantz, R. C. (1996) Agmatine, a bioactive metabolite of arginine. Production, degradation, and functional effects in the kidney of the rat, *J. Clin. Invest. 97*, 413−420.
14. Takemura, M., Kitanaka, N., and Kitanaka, J. (2003) Signal transduction by histamine in the cerebellum and its modulation by N-methyltransferase, *Cerebellum 2*, 39−43.
15. Schwartz, J. C., Arrang, J. M., Garbarg, M., Pollard, H., and Ruat, M. (1991) Histaminergic transmission in the mammalian brain, *Physiol. Rev. 71*, 1−51.
16. Burkard, W. P., Gey, K. F., and Pletscher, A. (1963) Diamine oxidase in the brain of vertebrates, *J. Neurochem. 10*, 183−186.
17. Preuss, C. V., Wood, T. C., Szumlanski, C. L., Raftogianis, R. B., Otterness, D. M., Girard, B., Scott, M. C., and Weinshilboum, R. M. (1998) Human histamine N-methyltransferase pharmacogenetics: Common genetic polymorphisms that alter activity, *Mol. Pharmacol. 53*, 708−717.
18. Chen, G. L., Wang, H., Wang, W., Xu, Z. H., Zhou, G., He, F., and Zhou, H. H. (2003) Histamine N-methyltransferase gene polymorphisms in Chinese and their relationship with enzyme activity in erythrocytes, *Pharmacogenetics 13*, 389−397.
19. Chen, G. L., Wang, W., Xu, Z. H., Zhu, B., Wang, L. S., Zhou, G., Wang, D., and Zhou, H. H. (2003) Genotype-phenotype correlation for histamine N-methyltransferase in a Chinese Han population, *Clin. Chim. Acta 334*, 179−183.
20. Chen, G. L., Xu, Z. H., Wang, W., Wang, G. P., Zhou, G., Wang, D., and Zhou, H. H. (2002) Analysis of the C314T and A595G mutations in histamine N-methyltransferase gene in a Chinese population, *Clin. Chim. Acta 326*, 163−167.
21. Scott, M. C., Van Loon, J. A., and Weinshilboum, R. M. (1988) Pharmacogenetics of N-methylation: Heritability of human erythrocyte histamine N-methyltransferase activity, *Clin. Pharmacol. Ther. 43*, 256−262.
22. Horton, J. R., Sawada, K., Nishibori, M., Zhang, X., and Cheng, X. (2001) Two polymorphic forms of human histamine methyltransferase: Structural, thermal, and kinetic comparisons, *Structure 9*, 837−849.
23. Girard, B., Otterness, D. M., Wood, T. C., Honchel, R., Wieben, E. D., and Weinshilboum, R. M. (1994) Human histamine N-methyltransferase pharmacogenetics: Cloning and expression of kidney cDNA, *Mol. Pharmacol. 45*, 461−468.
24. Price, R. A., Scott, M. C., and Weinshilboum, R. M. (1993) Genetic segregation analysis of red blood cell (RBC) histamine N-methyltransferase (HNMT) activity, *Genet. Epidemiol. 10*, 123−131.
25. Yan, L., Galinsky, R. E., Bernstein, J. A., Liggett, S. B., and Weinshilboum, R. M. (2000) Histamine N-methyltransferase pharmacogenetics: Association of a common functional polymorphism with asthma, *Pharmacogenetics 10*, 261−266.
26. Sasaki, Y., Ihara, K., Ahmed, S., Yamawaki, K., Kusuhara, K., Nakayama, H., Nishima, S., and Hara, T. (2000) Lack of association between atopic asthma and polymorphisms of the histamine H1 receptor, histamine H2 receptor, and histamine N-methyltransferase genes, *Immunogenetics 51*, 238−240.
27. Sharma, S., Mann, D., Singh, T. P., and Ghosh, B. (2005) Lack of association of histamine-N-methyltransferase (HNMT) polymorphisms with asthma in the Indian population, *J. Hum. Genet. 50*, 611−617.
28. Deindl, P., Peri-Jerkan, S., Deichmann, K., Niggemann, B., Lau, S., Sommerfeld, C., Sengler, C., Muller, S., Wahn, U., Nickel, R., and Heinzmann, A. (2005) No association of histamine-N-methyltransferase polymorphism with asthma or bronchial hyperresponsiveness in two German pediatric populations, *Pediatr. Allergy Immunol. 16*, 40−42.
29. Chen, G. L., Zhu, B., Nie, W. P., Xu, Z. H., Tan, Z. R., Zhou, G., Liu, J., Wang, W., and Zhou, H. H. (2004) Single nucleotide polymorphisms and haplotypes of histamine N-methyltransferase in patients with gastric ulcer, *Inflammation Res. 53*, 484−488.
30. Oroszi, G., Enoch, M. A., Chun, J., Virkkunen, M., and Goldman, D. (2005) Thr105Ile, a functional polymorphism of histamine N-methyltransferase, is associated with alcoholism in two independent populations, *Alcohol.: Clin. Exp. Res. 29*, 303−309.
31. Reuter, M., Jeste, N., Klein, T., Hennig, J., Goldman, D., Enoch, M. A., and Oroszi, G. (2006) Association of THR105Ile, a functional polymorphism of histamine N-methyltransferase (HNMT), with alcoholism in German Caucasians, *Drug Alcohol Depend*. (in press).
32. Horton, J. R., Sawada, K., Nishibori, M., and Cheng, X. (2005) Structural basis for inhibition of histamine N-methyltransferase by diverse drugs, *J. Mol. Biol. 353*, 334−344.
33. Levitt, M. (1990) *ENCAD: Energy Calculations and Dynamics, Computer Program*, Stanford University, Stanford, CA, and Yeda, Rehovot, Israel.
34. Beck, D. A. C., Alonso, D. O. V., and Daggett, V. (2004) *ilmm*, University of Washington, Seattle.
35. Beck, D. A., and Daggett, V. (2004) Methods for molecular dynamics simulations of protein folding/unfolding in solution, *Methods 34*, 112−120.
36. Levitt, M., Hirshberg, M., Sharon, R., and Daggett, V. (1995) Potential energy function and parameters for simulations of the molecular dynamics of proteins and nucleic acids in solution, *Comput. Phys. Commun. 91*, 215−231.
37. Levitt, M., Hirshberg, M., Sharon, R., Laidig, K. E., and Daggett, V. (1997) Calibration and testing of a water model for simulation of the molecular dynamics of proteins and nucleic acids in solution, *J. Phys. Chem. B 101*, 5051−5061.
38. Kell, G. S. (1967) Precise representation of volume properties of water at one atmosphere, *J. Chem. Eng. Data 12*, 66−69.
39. Hubbard, S. J., and Thorton, J. M. (1993) *NACCESS*, Department of Biochemicstry and Molecular Biology, University College, London.
40. Hunenberger, P. H., Mark, A. E., and van Gunsteren, W. F. (1995) Fluctuation and cross-correlation analysis of protein motions observed in nanosecond molecular dynamics simulations, *J. Mol. Biol. 252*, 492−503.
41. Rutherford, K., Bennion, B. J., Parson, W. W., and Daggett, V. (2006) The 108M polymorph of human catechol O-methyltrans-

ferase is prone to deformation at physiological temperatures, *Biochemistry 45*, 2178−2188.
42. Chen, J., Lipska, B. K., Halim, N., Ma, Q. D., Matsumoto, M., Melhem, S., Kolachana, B. S., Hyde, T. M., Herman, M. M., Apud, J., Egan, M. F., Kleinman, J. E., and Weinberger, D. R. (2004) Functional analysis of genetic variation in catechol-O-methyltransferase (COMT): Effects on mRNA, protein, and enzyme activity in postmortem human brain, *Am. J. Hum. Genet. 75*, 807−821.
43. Lotta, T., Vidgren, J., Tilgmann, C., Ulmanen, I., Melen, K., Julkunen, I., and Taskinen, J. (1995) Kinetics of human soluble and membrane-bound catechol O-methyltransferase: A revised mechanism and description of the thermolabile variant of the enzyme, *Biochemistry 34*, 4202−4210.
44. Shield, A. J., Thomae, B. A., Eckloff, B. W., Wieben, E. D., and Weinshilboum, R. M. (2004) Human catechol O-methyltransferase genetic variation: Gene resequencing and functional characterization of variant allozymes, *Mol. Psychiatry 9*, 151−160.
45. Goodman, J. E., Jensen, L. T., He, P., and Yager, J. D. (2002) Characterization of human soluble high and low activity catechol-O-methyltransferase catalyzed catechol estrogen methylation, *Pharmacogenetics 12*, 517−528.

BI701737F